Journal of
Applied Crystallography

ISSN 0021-8898Received 16 August 2002
Accepted 30 November 2006

Hierarchical bionanotubes formed by the self assembly of microtubules with cationic membranes or polypeptides

Uri Raviv,*‡ Daniel J. Needleman,¶ Kai K. Ewert and Cyrus R. Safinya*

Materials Department, Physics Department, and Molecular, Cellular, and Developmental Biology Department, University of California, Santa Barbara, CA 93106, USA. Correspondence e-mail: raviv@chem.ch.huji.ac.il, safinya@mrl.ucsb.edu

At present there is a surge in interest in biophysical research aimed at elucidating collective interactions between cellular proteins and associated biomolecules leading to supramolecular structures, with the ultimate goal of relating structure to function. The nerve cell cytoskeleton provides a rich example of highly ordered bundles and networks of interacting neurofilaments, microtubules and filamentous actin, where the nature of the interactions, structures and structure–function correlations remain poorly understood. We present synchrotron X-ray diffraction and electron microscopy data, in reconstituted protein systems from the bovine central nervous system, which reveal unexpected structures not predicted by current electrostatic theories. By mixing preassembled microtubules with charged membranes or polypeptides we found hierarchical bionanotubes made of microtubules coated by lipid bilayers or polypeptides, which in turn are coated with a third layer of tubulin oligomers forming rings or spirals.

1. Introduction

The interactions between lipids and biopolymers have been investigated in the past few years. In this paper we will describe a new paradigm for lipid self-assembly leading to nanotubule formation in mixed charged systems. We looked at the interaction between microtubules, negatively charged nanometer scale hollow cylinders derived from the eukaryotic cell cytoskeleton, and cationic lipid membranes and discovered, under the appropriate conditions, spontaneously forming lipid protein nanotubules. Before we address our subject we will describe earlier studies that looked at the lipid–biopolymer interactions.

When mixing cationic lipids and DNA, DNA–lipid complexes are formed and are used to deliver genes into cells (Koltover *et al.*, 1998). The complexes can be in the lamellar phase, composed of alternating DNA monolayers and lipid bilayers. When the spontaneous curvature of the lipids is negative a transition to inverted hexagonal phase occurs, at which the DNA molecules are coated by a lipid monolayer and arrange in a hexagonal array. The inverted hexagonal phase has a higher transfection efficiency, demonstrating that the structure of lipid–biopolyelectrolyte complexes may profoundly affect their function.

Both of these structures are similar to the original lipid bilayer phase, so the structures of the complexes are templated by the lipids. The reason for the complex formation is a net gain in entropy. We start with charged rods that have counterions that condense until the effective linear charge is one electron per Bjerrum length, which is about 7 Å in water. The membranes are also charged and most of their counterions are confined to a thin layer. When we mix the rods and the sheets, the charged rods and the charged membranes neutralize each other and all their counterions are released into solution, where each counterion gains about k_BT of solution entropy.

Polyelectrolyte lipid complexes (PLCs) that have been studied so far adopt mainly the multilamellar phase, which is templated by the original lipid symmetry, however different PLCs still exhibit various morphologies. Pinched multilamellar PLCs are obtained when poly(glutamic acid) (PGA), which is a negatively charged polypeptide with a charge density of about 6 e nm^{-3}, a diameter of 1 nm and a persistence length of 2 nm, is complexed with cationic membranes (Subramanian *et al.*, 2000). Flat (thermally fluctuating) multilamellar PLCs are obtained when lambda DNA, which has a negative charge density of about 2 e nm^{-3}, a diameter of 2.5 nm and a persistence length of 50 nm, is complexed with cationic membranes (Radler *et al.*, 1997). Swollen multilamellar PLCs, in which each lipid bilayer is coated from either sides by an oppositely charged hydrated polyelectrolyte monolayer, are obtained when filamentous actin (F-actin), which has a negative surface charge density of 0.3 e nm^{-3}, a diameter of 8 nm and a persistence length of 10 μm, is complexed with cationic membranes (Wong *et al.*, 2000). Moreover, within the polyelectrolyte layers that form on the cationic lipid membranes, the degree of order increases with increasing polymer diameter and rigidity. For PGA we get no order, DNA forms one dimensional crystals on the membranes, such that the spacing between the DNA rods is well defined, however the DNA rods can still slide with respect to each other. F-actin molecules are even more ordered and form two-dimensional crystals on the cationic membranes. All of these structures are templated by the original multilamellar phase of the lipid

‡ Present address: The Department of Physical Chemistry, The Institute of Chemistry, The Hebrew University of Jerusalem, Givat Ram, 91904, Jerusalem, Israel
¶ Present address: Harvard Medical School, Harvard University, Boston, MA, USA

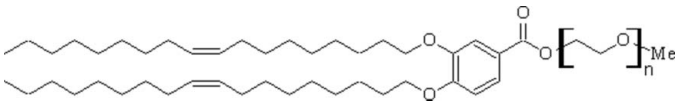

Figure 1
The chemical structure of the C18-mPEG2000 lipid used to remove the tubulin oligomers from the LPN structure; $n = 45$.

bilayers and the biopolymers just adsorb on the membranes and are incorporated between the membranes.

Microtubules (MTs) are net-negatively charged supramolecular polymers, which self-assemble from tubulin protein subunits into hollow cylinders. Tubulin dimers are arranged head to tail in protofilaments and form the MT wall. MTs are critical components in a broad range of functions in eukaryotic cells – from providing tracks for the transport of cargo to forming the spindle structure for chromosome segregation before cell division. They are used as nanometer scale tracks in neurons for the transport of neurotransmitter precursors and enzymes to synaptic junctions in nerve cell communication.

MTs have a charge density of 0.2 e nm^{-3}, an outer diameter of about 26 nm, inner diameter of about 16 nm and a persistence length of several millimeters. Therefore, MT represents an extreme case of polymer outer diameter and rigidity. Hence, to understand the interplay between electrostatic and elastic interactions governing the interactions between lipids and biopolymers, it was of interest to study the structures and interactions between MT and cationic lipid bilayers. Unlike in most of the other complexes, for which the membrane bending energy overcomes the electrostatic interactions, here the reverse holds and the MT forms the template for the complex structure.

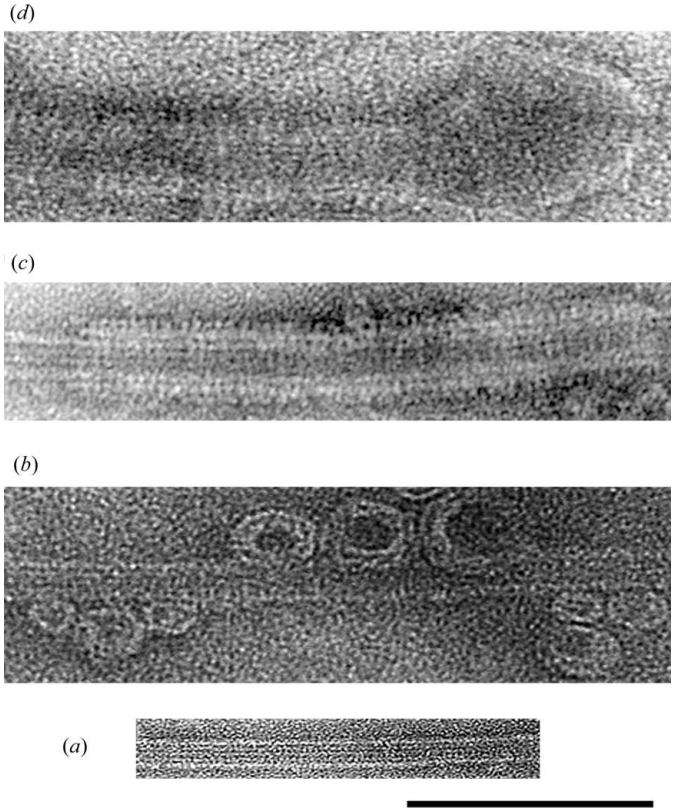

Figure 2
Transmission electron microscopy images of the various states described in the text. Whole mount images of liposomes–MT complexes, using DOTAP/DOPC solutions with $x_{CL} = N_{CL}/(N_{CL} + N_{NL})$ and $R_{CL/T} = N_{CL}/N_T$ values as follows. (*a*) pure MT. (*b*) MT–lipid complexes with $x_{CL} = 0.1$, $R_{CL/T} = 16$ showing the beads on a rod state. (*c*) The lipid protein nanotube (LPN) state with open ends, obtained with $x_{CL} = 0.5$ and $R_{CL/T} = 40$. (*d*) The LPN with closed ends obtained with $x_{CL} = 0.5$ and and $R_{CL/T} = 120$. Scale bar is 100 nm.

The second motivation to study the MT–lipid complexes is that they teach us about possible side effect of drug delivery treatment that are based on lipid–DNA complexes, where cationic lipids are introduced into cells and may interact with MTs. This study also provides insight into the assembly potential of MTs and tubulin.

Using synchrotron small-angle X-ray diffraction (SAXRD) and transmission electron microscopy (TEM), we found two novel structures (Raviv *et al.*, 2005; Raviv *et al.*, 2006). For low membrane charge density, we found that vesicles adsorb onto the MT and appear as 'beads on a rod' (BOR). This is the most trivial structure that can form when vesicles interact with polyelectrolytes and was previously hypothesized for cationic lipid–DNA complexes (Felgner *et al.*, 1987), but later was experimentally (Radler *et al.*, 1997; Koltover *et al.*, 1998) proven unstable. The BOR state, however, seems to be a kinetically trapped state. The ground state of the system follows the MT template and forms a lipid protein nanotube (LPN) structure, found with higher membrane charge densities and described below.

For membranes of low and intermediate rigidity, we found that the cationic liposomes spread and coat the MTs and the external lipid layer is decorated by tubulin oligomers, forming a novel LPN. By controlling the cationic lipid/tubulin stoichiometry, $R_{CL/T}$, of the complex, the LPN can switch between a state with open ends to a state with closed ends with lipid caps. This forms the basis for controlled drug encapsulation and release. Here we show that the third tubulin layer can be removed by adding to the membranes lipids with poly(ethylene glycol) PEG chains.

We then looked at the interactions between MT and the cationic polypeptide, poly L-lysine and found a similar structure: the poly L-lysine coats the MT and is then coated by a third layer of tubulin oligomers, forming a peptide–protein nanotube (PPN).

2. Experimental

Tubulin was purified from bovine brains, concentrated to 45 μ*M*, polymerized at 310 K and taxol-stabilized as described (Needleman *et al.*, 2004*b*; Raviv *et al.*, 2005). The cationic lipid used was dioleoyl($C_{18:1}$) trimethyl ammonium propane (DOTAP). The membrane charge density, σ, was adjusted by mixing a neutral lipid bearing the same hydrophobic tail but a phosphatidylcholine (PC) head group (DOPC) to the charged lipid. Equal volumes of MTs and liposome solutions were mixed and the resulting complexes were characterized by transmission electron microscopy (TEM) and SAXRD performed at Stanford Synchrotron Radiation Laboratory, beamline 4-2.

The mole fraction of cationic lipids in the membrane is given by

$$x_{CL} \equiv N_{CL}/(N_{CL} + N_{NL}), \quad (1)$$

where N_{CL} and N_{NL} are the numbers of cationic and neutral lipids, respectively. The relative cationic lipid/tubulin stoichiometry, $R_{CL/T}$, is defined as

$$R_{CL/T} \equiv N_{CL}/N_T, \quad (2)$$

where N_T is the number of tubulin dimers. $R_{CL/T} \sim 40$ is the mixing isoelectric point.

To remove the third tubulin layer a small percentage of C_{18}-mPEG2000 lipids {1,2-dioleoyl-*sn*-*glycero*-3-phosphoethanolamine-*N*-[poly(ethylene glycol)-2000], the mean number of monomers in the

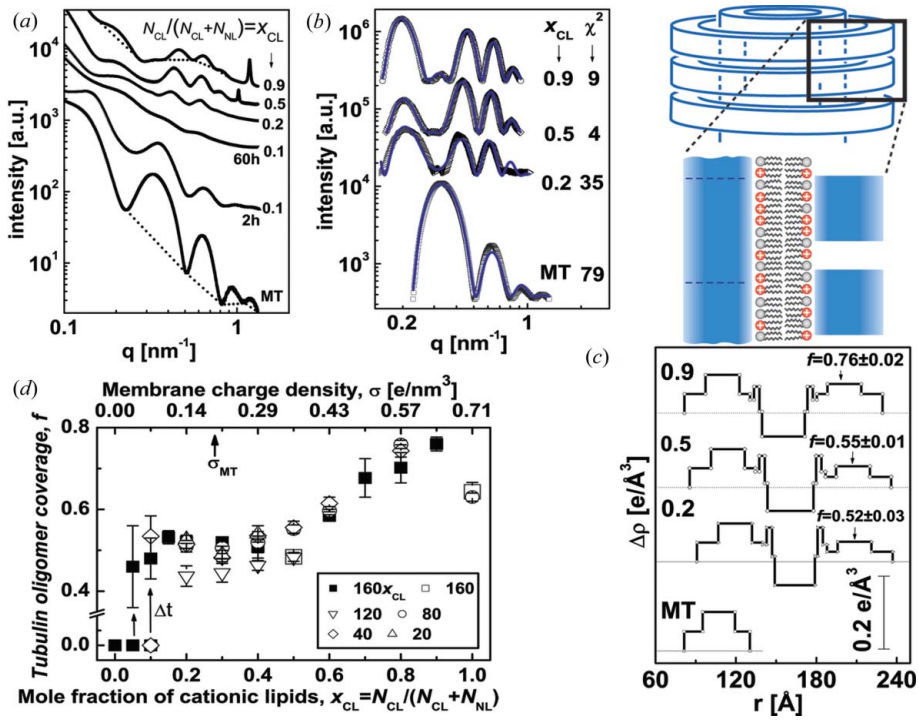

Figure 3
(*a*) Radially averaged scattering intensities of MTs and MT–lipid complexes (solid symbols), using DOTAP/DOPC solutions with $x_{CL} = N_{CL}/(N_{CL} + N_{NL})$ as indicated in the figure. $R_{CL/T} = N_{CL}/N_T$ is given by $R_{CL/T} = 160x_{CL}$, corresponding to the point at which the total amount of lipid is exactly enough to coat each MT with a bilayer. For $x_{CL} = 0.1$ two scans are shown, 2 h and 60 h after preparing the sample. The broken curves are examples of the assumed background (Andreu *et al.*, 1992; Fernando-Diaz *et al.*, 1996; Needleman *et al.*, 2004*b*). (*b*) Scattering data from (*a*), following background subtraction (open symbols). The solid curves are the fitted scattering models. Their χ^2 values are as in the figure. (*c*) The variation of the radial electron density, $\Delta\rho(r)$, relative to water (broken lines), of the MTs and complex walls, obtained from fitting the scattering data in (*b*) to models of concentric cylinders. r is the distance from the center of the cylinders. The values for the tubulin oligomer coverage f, as obtained from the nonlinear fit, are indicated on the right side. The schematic represents a perpendicular cut through the MT–membrane–tubulin complex wall, corresponding to $\Delta\rho(r)$. (*d*) State diagram: f as a function of x_{CL} or the membrane charge density, σ, when lipids can fully cover the MTs. Each data point is based on scattering data and models as in (*a*)–(*c*). Solid squares correspond to $R_{CL/T} = 160x_{CL}$. Open symbols represent different $R_{CL/T}$ values, as indicated in the figure. For $0 < x_{CL} \leq 0.1$ we initially get $f = 0$ (corresponding to the BOR structure). Over time ($\Delta t \sim 60$ h), we obtain LPNs with higher f values as indicated by the arrows.

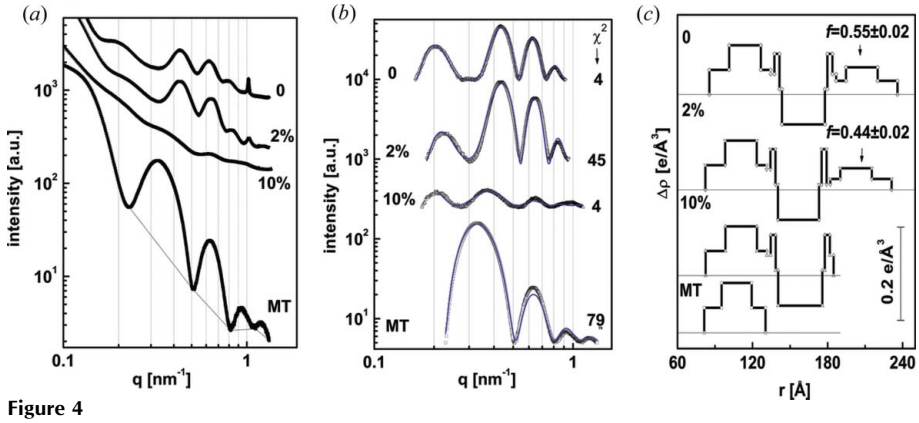

Figure 4
Synchrotron small-angle X-ray scattering data and analysis of LPN with C18 mPEG 2000 lipids. (*a*) Radially averaged scattering intensities of MTs and MT–lipid complexes (solid symbols), using DOTAP/(DOPC + C18mPEG2000) solutions with $x_{CL} = N_{CL}/(N_{CL} + N_{NL}) = 0.5$, with increasing C18mPEG 2000 percentage, as indicated in the figure. $R_{CL/T} = N_{CL}/N_T = 80$. The broken curve is an example of the assumed background (Andreu *et al.*, 1992; Fernando-Diaz *et al.*, 1996; Needleman *et al.*, 2004*b*). (*b*) Scattering data from (*a*), following background subtraction (open symbols). The solid curves are the fitted scattering models. Their χ^2 values are as in the figure. (*c*) The variation of the radial electron density, $\Delta\rho(r)$, relative to water (broken lines), of the MTs and complex walls, obtained from fitting the scattering data in (*b*) to models of concentric cylinders. r is the distance from the center of the cylinders. The values for the tubulin oligomer coverage, f, obtained from the nonlinear fit are indicated on the right side.

poly(ethylene glycol) unit <*n*> = 452802 mol wt.} was added, synthesized as described (Martin-Herranz *et al.*, 2004). Its chemical structure is shown in Fig. 1. We also used poly L-lysine (Sigma) of molecular weight 260 kD at concentration of 0.5 μ*M*.

3. Results and discussion

A set of TEM images covering the structures in the phase diagram of MT–membrane complexes are shown in Fig. 2. As a control, an image of MT is shown in Fig. 2(*a*). For cationic lipid mole fraction $x_{CL} = 0.1$, we initially find the weakly positive charged vesicles ('beads') adsorbed onto the negatively charged microtubule, MT, wall ('rod'), forming the beads on a rod, BOR structure [Fig. 2(*b*)]. This state is, however, kinetically trapped: over longer times, ~60 h, the adsorbed vesicles 'wet' the MT surface, forming the lipid–protein nanotube, LPN. For $x_{CL} > 0.1$ the LPN forms immediately upon mixing [Figs. 2(*c*) and (*d*)]. The images reveal that the LPN is made of three layers: Intact MTs are coated by a lipid bilayer (appears brighter in the images, as the ionic stain avoids the hydrophobic lipid tails), which in turn are coated by tubulin oligomers forming rings or spirals. The oligomer orientation is perpendicular to the internal MT protofilament direction and their density increases with x_{CL}. The three layered LPN structure arises because of the mismatch between the charge densities of MTs and cationic membranes. The oligomers coat the external lipid monolayer to optimize the electrostatic interactions and counterion release.

At a given mole fraction of cationic lipids, x_{CL}, when the total MT surface area exceeds the total membrane area, the MTs are only partially coated [Fig. 2(*c*), $x_{CL} = 0.5$ and cationic lipid/tubulin stoichiometry, $R_{CL/T} = 40$], forming LPNs with open ends. When the reverse is true, some of the excess vesicles are attached primarily to the ends of the LPNs [Fig. 2(*d*), $x_{CL} = 0.5$, $R_{CL/T} = 120$], forming LPNs with closed ends with lipid caps. The oligomer density at a given x_{CL} is similar for both open and closed LPNs.

TEM images and SAXRD measurements performed on pure MT solutions [Figs. 2(*a*) and 3] are in agreement with earlier studies (Li *et al.*, 2002; Andreu *et al.*, 1992; Fernando-Diaz *et al.*, 1996; Needleman *et al.*, 2004*a*; Needleman *et al.*, 2004*b*; Raviv *et al.*, 2005; Needleman *et al.*, 2005*b*; Needleman *et al.*, 2005*a*; Raviv *et al.*, 2006). The SAXRD profile of MTs [Fig. 3(*a*)] is consistent with the form factor of isotropic hollow cylinders

[Fig. 3(*b*)]. Based on MT structural data (Li *et al.*, 2002; Lee *et al.*, 1973), we modeled the MT as three concentric cylindrical shells, of a high electron density region surrounded by two low ones, as shown in Fig. 3(*c*), keeping the total wall thickness and mean electron density as those of MTs. The thickness and location of the high electron density region, within the MT wall, and the inner MT radius are fitting parameters in this model [see appendix of Raviv *et al.* (2007) for details].

A set of SAXRD data for MT–lipid (DOTAP/DOPC) complexes is shown in Fig. 3(*a*), where the intensity is plotted as a function of the modulus of the scattering vector q, defined as $q = (4\pi/\lambda)\sin\theta$, where $\lambda = 0.154$ nm is the X-ray photon wavelength and θ is half the scattering angle. For $x_{CL} > 0.1$, the SAXRD scans show broad oscillations that are different from that of MTs and correspond to the form factor of the LPNs. For $x_{CL} = 0.1$, 2 h after MTs and membranes were mixed, the SAXRD scan is consistent (for $q > 0.2$ nm^{-1}) with the form factor of isotropic MT solutions. The SAXRD scan in Fig. 3*a* is therefore consistent with the BOR state [shown by the TEM image in Fig. 2(*b*)]. SAXRD scans taken 60 h after mixing (Fig. 3*a*) show that this structure slowly evolves into the form factor of the LPNs.

To gain quantitative insight into the organization of the complexes, the background-subtracted SAXRD data, shown in Fig. 3(*b*), was analyzed by fitting to a model (see appendix of reference (Raviv *et al.*, 2007) for details). To model the data, a series of power laws that pass through the minima of the scattering intensities was subtracted. This was done in earlier MT-related scattering studies (Needleman *et al.*, 2004*b*; Fernando-Diaz *et al.*, 1996; Andreu *et al.*, 1992; Raviv *et al.*, 2005) and represent the assumed background scattering. This assumption is good for narrow size distribution. The isotropic concentric cylindrical shells model of MTs was extended to include the second lipid bilayer and the third tubulin layer [Fig. 3(*c*)]. The radial electron density profile of the inner MT wall and outer tubulin monolayer are based on the fit to the MT scattering data. The parameters for the electron density profile of the lipid bilayer are based on literature data (Liu & Nagle, 2004; Wong *et al.*, 2000). Finally, the third tubulin layer was multiplied by the fraction, f, of tubulin coverage relative to the inner MT wall. f is the unknown parameter in this model and was allowed to float freely. The scattering models [Fig. 3(*b*)] fit very well to the data.

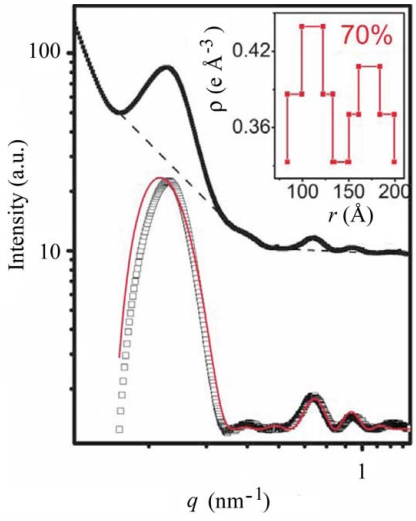

Figure 5
Synchrotron small-angle X-ray scattering data and analysis of MT complexed with 0.5 μ*M* of poly L-lysine 260 kD. Upper solid symbols: Radially averaged scattering intensities of MT complexed with poly L-lysine. The broken curve is the assumed background (Andreu *et al.*, 1992; Fernando-Diaz *et al.*, 1996; Needleman *et al.*, 2004*b*). Lower open symbols: scattering data of the upper solid symbols following background subtraction. The lower solid curve is the fitted scattering model. The inset shows the variation of the radial electron density, $\Delta\rho(r)$, relative to water of the complex wall, obtained from fitting the scattering data to models of concentric cylinders. r is the distance from the center of the cylinders. The tubulin oligomer coverage, f, obtained from the nonlinear fit is 0.7, as indicated on the right. The +/− charge ratio is 1:2.

Fig. 3(*d*) summarizes a series of SAXRD scans from Fig. 3(*a*), analyzed as in Fig. 3(*b* and *c*). A states diagram is obtained, in which f is plotted as a function of x_{CL} or the membrane charge density, σ, at various $R_{CL/T}$ values. For $x_{CL} = 0$, corresponding to pure DOPC membrane, SAXRD scans show only the isotropic MT form factor. This state (indicated as $f = 0$) is stable for days, indicating that the LPN is induced by the cationic lipids. At $0 < x_{CL} \leq 0.1$, we have kinetically trapped states of BOR and bridging (also indicated by $f = 0$) that evolve slowly into the LPN. For $x_{CL} > 0.1$, we only see the LPN with f values that increase monotonically with x_{CL}. $R_{CL/T}$ has little effect on f, in agreement with the TEM images (Fig. 2).

We then studied how the incorporation of neutral lipids with similar lipid tail but with a PEG chain attached to the head group influences the structure of the LPN. In Fig. 4(*a*), we show SAXRD scans of LPN with $x_{CL} = 0.5$ and cationic lipid/tubulin stoichiometry $R_{CL/T} = 80$, with increasing percentage of C18-mPEG 2000 lipids. A clear change in the form factor is observed as we add more of the C18-mPEG 2000 lipids. We analyzed the background subtracted SAXRD data, shown in Fig. 4(*b*), by fitting to a similar model shown in Fig. 3. We find that, as we increase the amount of PEG lipids, the fraction f of tubulin coverage relative to the inner MT wall decreases from 55% (with no added C18-mPEG 2000 lipids) to no coverage when 10 mol% of C18-mPEG 2000 lipid is added to the membrane. The reason for the removal of the third tubulin layer is the increasing excluded volume occupied by the PEG chains that are coating the outer lipid monolayer forming the LPN. Since in principle one can attach various end groups to the PEG chains, this result forms the basis for functionalizing the LPN complex for targeted drug delivery.

To gain further insight into the formation of the LPN, we examined the complexation of MT with other polycations. We studied the interactions between MT and the cationic polypeptide poly L-lysine. In Fig. 5 we show SAXRD data of the MT–poly L-lysine complexes. The data shows a new type of form factor which is different from the MT form factor and the LPN form factor. Following a background subtraction similar to that described above, we fitted the data to an isotropic concentric cylindrical shells model of MT coated with a 1 nm thick polymer layer, which in turn is coated by a third tubulin wall. As in the LPN complexes, the radial electron density profile of the inner MT wall and outer tubulin monolayer are based on the fit to the MT scattering data. The electron density profile of the confined polypeptide is assumed to be uniform. Finally, the third tubulin layer is multiplied by the fraction, f, of tubulin coverage relative to the inner MT wall. From the fit to the data we find $f = 0.7$, which is consistent with the relatively high charge density of the poly L-lysine (1 e 0.3 nm^{-1}). The +/− charge ratio was 1:2. In Fig. 6 we show a TEM image of the complex, which is in agreement with the SAXRD data.

The similarity between the LPN and the peptide–MT complex shows that the formation of the third tubulin wall is not specific to the lipids. Rather, it is driven by the optimization of the electrostatic interactions between the cationic lipid membranes (or the cationic polypeptides) and the protein. However, the formation of a third layer does require the presence of a polycation. We have shown (Needleman *et al.*, 2004*b*) that the assembly between MT and simple counterions leads to other phases: tightly packed hexagonal bundles with controllable diameters are observed for tri-, tetra-, and penta-

Figure 6
Transmission electron microscopy images of MT complexed with 0.5 μ*M* of poly L-lysine 260 kD. Scale bar is 100 nm.

valent counterions (such as Spermidine 3+, Spermine 4+ and Lys 5+). Unexpectedly, in the presence of small divalent cations (such as Mg^{2+}), we have discovered a living necklace bundle phase, comprised of dynamical assemblies of MT nematic membranes with linear, branched, and loop topologies. The morphologically distinct MT assemblies give insight into general features of bundle formation and may be used as templates for miniaturized materials with applications in nanotechnology and biotechnology.

The work was performed using synchrotron X-ray scattering techniques at the Stanford Synchrotron Radiation Laboratory (SSRL) at beamline 4-2, combined with electron microscopy at the University of California, Santa Barbara, USA. This project is supported by grants NSF DMR-0503347, CTS-0404444, and NIH GM-59288 and NS-13560. The Stanford Synchrotron radiation laboratory is supported by the US DOE. UR acknowledges the support of the International Human Frontier Science Program Organization and the European Molecular Biology Organization.

References

Andreu, J. M., Bordas, J., Diaz, J. F., Garcia de Ancos, J., Gil, R., Medrano, F. J., Nogales, E., Pantos, E. & Towns-Andrews, E. (1992). *J. Mol. Biol.* **226**, 169–184.
Felgner, P. L., Gadek, T. R., Holm, M., Roman, R., Chan, H. W., Wenz, M., Northrop, J. P., Ringold, G. M. & Danielsen, M. (1987). *Proc. Natl Acad. Sci. USA*, **84**, 7413–7417.
Fernando-Diaz, J., Andreu, J. M., Diakun, G., Towns-Andrews, E. & Bordas, J. (1996). *Biophys. J.* **70**, 2408–2420.
Koltover, I., Salditt, T., Radler, J. O. & Safinya, C. R. (1998). *Science*, **281**, 78–81.
Lee, J. C., Frigon, R. P. & Timasheff, S. N. (1973). *J. Biol. Chem.* **248**, 7253–7262.
Li, H., DeRosier, D. J., Nickolson, W. V., Nogales, E. & Downing, K. H. (2002). *Structure*, **10**, 1317–1328.
Liu, Y. F. & Nagle, J. F. (2004). *Phys. Rev. E*, **69**, 040901.
Martin-Herranz, A., Ahmad, A., Evans, H. M., Ewert, K., Schulze, U. & Safinya, C. R. (2004). *Biophys. J.* **68**, 1160–1168.
Needleman, D. J., Jones, J. B., Raviv, U., Ojeda-Lopez, M. A., Miller, H. P., Wilson, L. & Safinya, C. R. (2005*a*). *J. Phys. Cond. Matter*, **17**, S3225–S3230.
Needleman, D. J., Ojeda-Lopez, M. A., Raviv, U., Ewert, K., Jones, J. B., Miller, H. P., Wilson, L. & Safinya, C. R. (2004*a*). *Phys. Rev. Lett.* **93**, 198104–198101.
Needleman, D. J., Ojeda-Lopez, M. A., Raviv, U., Ewert, K., Jones, J. B., Miller, H. P., Wilson, L. & Safinya, C. R. (2005*b*). *Biophys. J.* **89**, 3410–3423.
Needleman, D. J., Ojeda-Lopez, M. A., Raviv, U., Miller, H. P., Wilson, L. & Safinya, C. R. (2004*b*). *Proc. Natl Acad. Sci. USA*, **101**, 16099–16103.
Radler, J. O., Koltover, I., Salditt, T. & Safinya, C. R. (1997). *Science*, **275**, 810–814.
Raviv, U., Needleman, D. J., Li, Y., Miller, H. P., Wilson, L. & Safinya, C. R. (2005). *Proc. Natl Acad. Sci. USA*, **102**, 11167–11172.
Raviv, U., Needleman, D. J. & Safinya, C. R. (2006). *J. Phys. Cond. Matter*, **18**, S1271–S1279.
Raviv, U., Nguyen, T., Ghafouri, R., Needleman, D. J., Li, Y., Miller, H. P., Wilson, L., Bruinsma, R. F. & Safinya, C. R. (2007). *Biophys. J.* **92**, 278–287.
Subramanian, G., Hjelm, R. P., Deming, T. J., Smith, G. S., Li, Y. & Safinya, C. R. (2000). *J. Am. Chem. Soc.* **122**, 26–34.
Wong, G. C. L., Tang, J. X., Lin, A., Li, Y., Janmey, P. A. & Safinya, C. R. (2000). *Science*, **288**, 2035–2039.